Heavy-Atom-Free Bay-Substituted Perylene Diimide Donor-Acceptor Photosensitizers

Deckers, Jasper; Cardeynaels, Tom; Lutsen, Laurence; Champagne, Benoît; Maes, Wouter

Published in:
ChemPhysChem

DOI:
10.1002/cphc.202100269

Publication date:
2021

Heavy-Atom-Free Bay-Substituted Perylene Diimide Donor-Acceptor Photosensitizers

Jasper Deckers[+],[a, b] Tom Cardeynaels[+],[a, b, c] Laurence Lutsen,[b] Benoît Champagne,[c] and Wouter Maes*[a, b]

Perylene diimide (PDI) dyes are extensively investigated because of their favorable photophysical characteristics for a wide range of organic material applications. Fine-tuning of the optoelectronic properties is readily achieved by functionalization of the electron-deficient PDI scaffold. Here, we present four new donor-acceptor type dyads, wherein the electron donor units – benzo[1,2-*b*:4,5-*b'*]dithiophene, 9,9-dimethyl-9,10-dihydroacridine, dithieno[3,2-*b*:2',3'-*d*]pyrrole, and triphenylamine- are attached to the bay-positions of the PDI acceptor. Intersystem crossing occurs for these systems upon photoexcitation, without the aid of heavy atoms, resulting in singlet oxygen quantum yields up to 80% in toluene solution. Furthermore, this feature is retained when the system is directly irradiated with energy corresponding to the intramolecular charge-transfer absorption band (at 639 nm). Geometrical optimization and (time-dependent) density functional theory calculations afford more insights into the requirements for intersystem crossing such as spin-orbit coupling, dihedral angles, the involvement of charge-transfer states, and energy level alignment.

1. Introduction

Perylene-3,4:9,10-bis(dicarboximide)s, shortly perylene diimides (PDIs), are mostly known as vat dyes, but they are also frequently encountered as (parts of) functional organic materials for a wide range of optoelectronic applications such as (bio) molecular imaging, supramolecular photosystems, photonics, transistors, organic light-emitting diodes, and photovoltaics.[1] Due to their high molar extinction coefficients, fluorescence quantum yields (Φ_f) approaching unity, high (photo)stability, chemical robustness, and broad functionalization scope, PDIs are the most intensively studied members of the polycyclic aromatic hydrocarbon family.[2] Even more, solubility properties are easily tuned through variation of the imide substituents, while the electron-deficient PDI core is particularly suitable to alter the fluorescence and optoelectronic properties.[3]

The high Φ_f of PDI dyes results from their rigid and planar structure in combination with a low-lying triplet energy level. Furthermore, transfer of the excitons from a localized singlet (^{1}LE) to a triplet (^{3}LE) excited state, *i.e.* intersystem crossing (ISC), is unlikely (triplet quantum yields, $\Phi_T < 0.001$).[4] To enhance the ISC efficiency, bromine, iodine, or transition metal atoms have been readily employed to increase spin-orbit coupling (SOC) through the heavy-atom effect.[5] The increased ISC renders these compounds attractive as organic triplet photosensitizers (PSs), with broad applicability in photocatalysis, photovoltaics, triplet-triplet annihilation upconversion, and photodynamic therapy (PDT).[6] However, correlated drawbacks include shortened triplet state lifetimes, increased dark cytotoxicity, and additional synthetic efforts (and related costs).[7] Hence, heavy-atom-free ISC has gained increasing attention and various ISC mechanisms have been unraveled, such as exciton coupling, the use of spin converters, energy level matching, n-π*→π-π* transitions, radical-enhanced ISC, and charge-recombination (CR) induced ISC.[6,8] In this regard, several heavy-atom-free PDI systems with increased triplet populations have been developed over the years.[9]

For the presented study, we have based our molecular design on one specific form of CR-induced ISC, *i.e.* spin-orbit charge-transfer ISC (SOCT-ISC). Herein, enhanced ISC is observed for orthogonal dimers and dyads with a small separation distance between the donor (electron-rich) and acceptor (electron-poor) parts. The straightforward molecular design renders such systems synthetically more appealing, and the mechanism is already known in anthracene, acridinium, BODIPY, and perylene systems.[8,10] In these donor-acceptor dyads, photoinduced electron transfer (PET) results in the occupation of a charge-transfer (CT) state. If electronic coupling between the donor and acceptor is strong, the energy difference between this polar excited ^{1}CT state and the ^{3}LE state is small and 'back-electron' transfer into the localized triplet state is possible. Although CT state formation is widely observed for bay-functionalized PDI materials through CT state absorbance and/or fluorescence and accompanied fluorescence quenching, ISC has barely been investigated in more detail for these systems.[11] Only two examples of SOCT-ISC were recently reported. Barbon and coworkers developed carbazole-PDI dyads

[a] J. Deckers,[+] Dr. T. Cardeynaels,[+] Prof. W. Maes
UHasselt-Hasselt University, Institute for Materials Research (IMO), Design & Synthesis of Organic Semiconductors (DSOS), Agoralaan, 3590 Diepenbeek, Belgium
E-mail: wouter.maes@uhasselt.be
[b] J. Deckers,[+] Dr. T. Cardeynaels,[+] Dr. L. Lutsen, Prof. W. Maes
IMEC, Associated Lab IMOMEC, Wetenschapspark 1, 3590 Diepenbeek, Belgium
[c] Dr. T. Cardeynaels,[+] Prof. B. Champagne
UNamur-University of Namur, Laboratory of Theoretical Chemistry (LTC), Theoretical and Structural Physical Chemistry Unit, Namur Institute of Structured Matter, Rue de Bruxelles 61, 5000 Namur, Belgium
[+] These authors contributed equally.

Supporting information for this article is available on the WWW under https://doi.org/10.1002/cphc.202100269

with the carbazole donor attached to one of the two imide positions,[9t] while Fedin *et al.* chose to functionalize a bay-position with a weakly donating anthracene moiety.[9w]

To further explore this field, different bay-substituted donor-PDI dyads were synthesized here and their possible use as triplet PSs was evaluated by monitoring their singlet oxygen ($^1O_2$) generation abilities. We found moderate values for 9,9-dimethyl-9,10-dihydroacridine and dithieno[3,2-*b*:2′,3′-*d*]pyrrole donors, whereas the combination with benzo[1,2-*b*:4,5-*b*′] dithiophene resulted in high $^1O_2$ quantum yields ($\Phi_\Delta = 0.80$ in toluene). To broaden the possible application fields of these PSs, ISC was also evaluated in the red wavelength region. Toward application in PDT, this feature is essential as longer wavelengths reduce light scattering, minimize background signals from autofluorescence of biomolecules, and strongly enhance the penetration depth of the incident light beam.[12] Upon direct excitation into the dyads' CT states, the donor-PDI molecules retained their capability for $^1O_2$ generation. Although no perfect orthogonality was observed between the donor and acceptor parts of the dyes through quantum-chemical analysis, we found that a proper energy level alignment of the CT state with a higher triplet excited state of different nature facilitates the ISC process.

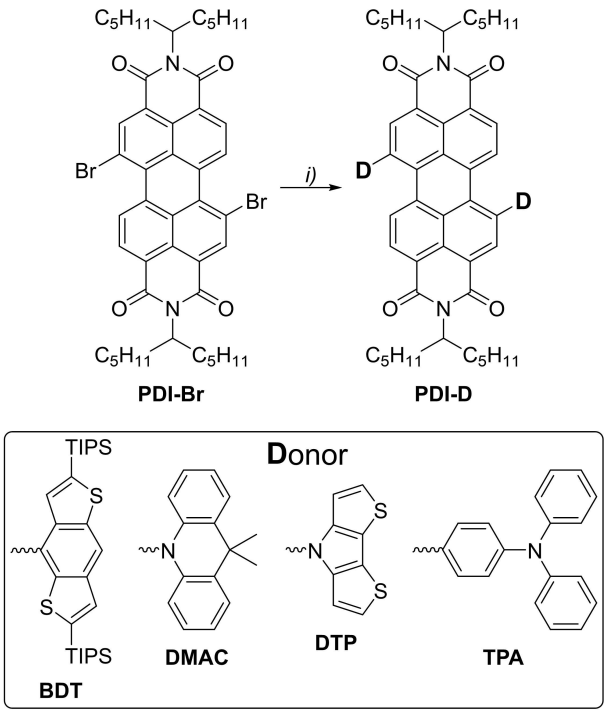

Scheme 1. Synthesis of **PDI-BDT**, **PDI-DMAC**, **PDI-DTP**, and **PDI-TPA** (showing only the most abundant 1,7-disubstituted regioisomers): i) Suzuki cross-coupling (**D**-pinacol, $Pd(PPh_3)_4$, K_2CO_3, *N*,*N*-dimethylformamide, inert atm, 24 h at 130 °C) or Buchwald-Hartwig amination (**D**, $Pd(OAc)_2$, $[(t\text{-}Bu)_3PH]BF_4$ (DMAC) or BINAP (DTP), NaO*t*Bu, dry toluene, inert atm, 24 h at 120 °C).

2. Results and Discussion

2.1. Structural Design and Synthesis

Synthesis of the PDI dyads started from commercially available perylene-3,4,9,10-tetracarboxylic dianhydride, which was treated with undecane-6-amine at elevated temperature to yield a symmetrically N,N′-substituted PDI (as described in literature).[1j] Long alkyl chains were chosen as imide substituents to limit π-π stacking and to improve solubility without affecting the optoelectronic properties too much. To tailor the photophysical properties of the PDI core, substitution of the bay-positions was performed with four different electron donor moieties of varying donor strength (Scheme 1), *i.e.* triisopropylsilyl (TIPS) substituted benzo[1,2-*b*:4,5-*b*′]dithiophene (**BDT**), 9,9-dimethyl-9,10-dihydroacridine (**DMAC**), dithieno[3,2-*b*:2′,3′-*d*]pyrrole (**DTP**), and triphenylamine (**TPA**). The **DMAC** and **TPA** donor units were chosen based on their ability to strengthen the vibronic coupling between excited triplet states via donor-acceptor vibrations over the C–N bond, thereby improving the (reversed) ISC abilities of fluorophores, as demonstrated in recent literature on organic emitters showing thermally activated delayed fluorescence (TADF).[13] The **BDT** donor unit was recently introduced by our group and was found to improve ISC from the singlet to the triplet excited state, likely due to the presence of the slightly heavier sulfur atoms.[14] **DTP** was introduced here as a novel electron-rich building block (taken from the field of organic photovoltaics[15]) that combines the features of the above two types of donor units as it comprises the possibility for C–N donor-acceptor bond formation and contains the heavier sulfur atoms. Because of the PDI's strong electron-accepting properties, the combination with a donor introduces CT character in the resulting donor-acceptor-donor molecules. This approach not only leads to long-wavelength CT emission, thereby pushing the emission into the near-infrared (NIR), but these CT states can also play an essential role in ISC *via* the SOCT-ISC mechanism.[8b]

To introduce the donor units, bromination was first performed at the bay-positions.[16] According to ^1H NMR analysis, two regioisomers were formed, a 1,7- and 1,6-dibrominated variant, in a 3:1 ratio (Figure S10).[17] We were unable to separate these isomers *via* column chromatography and the mixture was hence used further as such. The introduction of the donor moieties proceeded *via* Buchwald-Hartwig amination (**DMAC**, **DTP**) or Suzuki cross-coupling reactions (**BDT**, **TPA**). Details on the synthetic procedures and all characterization data are provided in the supporting information (SI). Purification *via* column chromatography and subsequently by size exclusion chromatography did not allow to separate the formed regioisomers and a similar 3:1 ratio of the 1,7- and 1,6-substituted isomers was obtained for all donor-PDI dyads (again based on ^1H NMR analysis; see SI). A twisted relation between the donor and acceptor subunits was envisioned due to the sterically hindered bay-positions. Although the exact structural requirements for SOCT-ISC are still under debate, orthogonality between the donor and acceptor moieties is important as the change in molecular orbital angular momentum will compensate for the change in electron spin angular momentum during triplet formation.[18]

2.2. Quantum Chemical Analysis

To analyze the structural parameters of the donor-PDI series, density functional theory (DFT) geometry optimizations were performed using the M06 exchange-correlation functional and the 6-311G(d) basis set. Vibrational analysis confirmed that all geometries correspond to minima on the potential energy surfaces. For **PDI-BDT**, the TIPS groups were omitted from the calculations to reduce the computational cost. This is acceptable because the TIPS groups pose little steric hindrance to the PDI core since they are positioned on the BDT α-positions and are facing away from the core. Furthermore, the electronic influence of the TIPS groups is deemed negligible due to the similar electronegativities for silicon and carbon and the fact that in prior work it was shown that delocalization of the highest occupied molecular orbital (HOMO) on the BDT unit did not extend onto the TIPS groups.[14] The quantum-chemical analysis was performed for both the 1,7- and 1,6-disubstituted PDI dyads. Both regioisomers showed similar properties, as was previously reported for disubstituted PDIs.[19] Since the 1,7-disubstituted PDIs are the most abundant species here, only their properties are discussed below. The results for the 1,6-disubstituted isomers are provided in the SI for completeness. From the optimized geometries (Figure 1), it is apparent that the donor and acceptor units have a considerable mutual steric hindrance, leading to large dihedral angles between the push and pull subunits (Table 1; 53–76°). The lowest unoccupied molecular orbital (LUMO) is localized on the PDI core for all compounds, whereas the HOMO is predominantly localized on the donor units (Figure 1). For **PDI-BDT** and **PDI-TPA**, there is also some delocalization of the HOMO onto the PDI core. Despite having a smaller donor-acceptor dihedral angle, the HOMO orbital for **PDI-DTP** does not delocalize onto the PDI core, likely because of poor overlap between the molecular

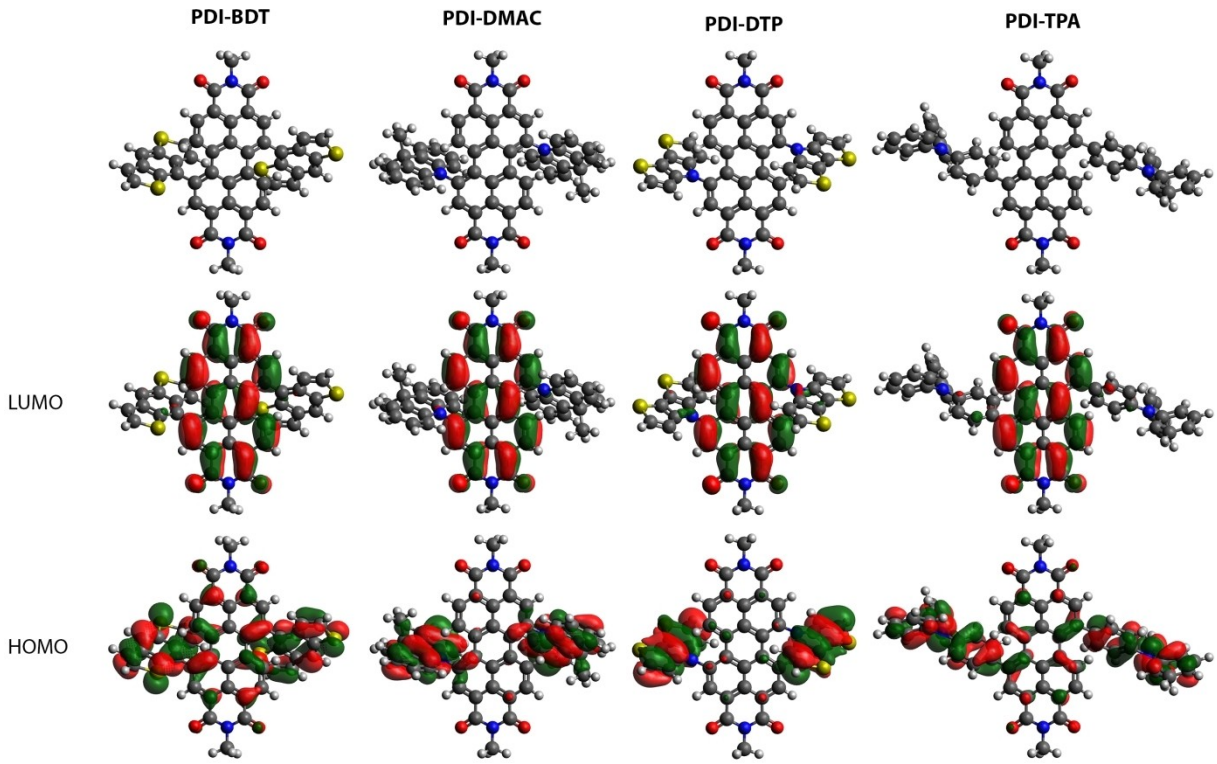

Figure 1. Optimized geometries and frontier molecular orbitals for all donor-PDI compounds in toluene solution as obtained using DFT calculations with LC-BLYP ($\omega = 0.17$ bohr^{-1})/6-311G(d) and the polarizable continuum solvation model. Isosurface values of 0.02 a.u. were used for all orbitals.

Table 1. Calculated vertical singlet (S_1 and S_2) and triplet (T_1 and T_2) excitation energies and their corresponding oscillator strengths for all donor-acceptor compounds using toluene as the solvent. The dihedral angles between the donor units and the PDI core are also given.

PDI	$S_0 \rightarrow S_1$			$S_0 \rightarrow S_2$		$S_0 \rightarrow T_1$	$S_0 \rightarrow T_2$	$T_2 \rightarrow S_1$	θ [°][d]
	ΔE [eV][a]	λ [nm][a]	Osc. Str.[b]	ΔE [eV][a]	Osc. Str.[b]	ΔE [eV][a]	ΔE (eV)[a]	ΔE (eV)[c]	
BDT	2.20	562	0.258	2.35	0.005	1.56	2.25	0.05	62
DMAC	1.76	706	0.050	1.80	0.001	1.52	1.76	<0.01	76
DTP	2.20	565	0.092	2.22	0.000	1.54	2.18	-0.02	60
TPA	2.14	580	0.461	2.42	0.030	1.47	2.25	0.11	53

[a] Vertical excitation energy/wavelength. [b] Oscillator strength. [c] Taken as the difference between the vertical excitation energy for the $S_0 \rightarrow T_2$ and the $S_0 \rightarrow S_1$ transition. [d] Averaged dihedral angle between the donor and acceptor units.

orbitals of the PDI and DTP units. Clear separation of the HOMO and LUMO in all cases points toward CT type HOMO-LUMO transitions for these compounds. Furthermore, the PDI cores are slightly deviated from planarity by incorporating the bay substituents, as observed by others previously (Figure S1).[1a]

To probe the excited state properties of the novel series of donor-PDI compounds, time-dependent DFT (TDDFT) calculations were performed using a modified LC-BLYP exchange-correlation functional in which the range-separating parameter ω has been changed to 0.17 bohr^{-1}. This was used in conjunction with the 6-311G(d) basis set and the polarizable continuum model (PCM) in toluene and chloroform to simulate apolar and more polar surroundings (Table 1, S7). The modified LC-BLYP ($\omega = 0.17$ bohr^{-1}) functional has been shown to perform well for donor-acceptor type molecules exhibiting strong CT character and is therefore believed to give a good representation of the excited state properties for these materials as well.[20]

The vertical excitation energies in toluene vary from 1.76 eV (706 nm) to 2.20 eV (562 nm) (Table 1). These data indicate that **DMAC** is the strongest donor unit, followed by **TPA**, **DTP**, and **BDT**. The oscillator strengths follow the trends observed for the HOMO and LUMO topologies, *i.e.* the compounds with a higher degree of HOMO-LUMO overlap give the largest oscillator strengths for the first singlet excited state (S_1) (Table 1). This is a direct consequence of the HOMO→LUMO character for the S_1 of all compounds (Table 2). The second singlet (S_2) excitation, which has HOMO-1→LUMO character, has an energy that is only slightly higher than the first vertical excitation energy. Notably, in the cases of **PDI-DMAC** and **PDI-DTP**, the difference is only 0.04 and 0.02 eV, respectively. The first triplet (T_1) excitation energy is significantly below that of S_1, at around 1.5 eV for all compounds. The second triplet (T_2) excitation energy is approximately similar to the S_1 excitation energy for all compounds. The energy difference is very small or even negligible for **PDI-BDT**, **PDI-DMAC**, and **PDI-DTP. PDI-TPA** shows a slightly larger difference between the T_2 and S_1 energies (0.11 eV).

The CT character of the various transitions was probed by looking at the differences between the excited and ground state electron densities according to the work of Le Bahers *et al.*[21] Here, the amount of charge transferred (q_{CT}) is used to characterize the degree of CT (Table 2). The q_{CT} values range from 0 to 1, with 1 being a full electron transferred from the donor to the acceptor. In some cases, the value is larger than 1, which is attributed by Le Bahers *et al.* to the size of the integration volume over which the density is integrated and is defined by the script rather than through manual input.[21] As can be seen from Table 2, the transitions from the ground state to S_1, S_2, and T_2 are of CT character, as indicated by the q_{CT} values close to 1. The q_{CT} values for $S_0 \rightarrow S_1$ of **PDI-BDT** and **PDI-TPA** are somewhat lower because of the increased overlap between the HOMO and LUMO, as pointed out earlier. The first triplet excited state of all donor-PDI compounds is of localized excited (LE) state character as it shows relatively small values for q_{CT} in comparison to the other excited states. These assignments can be visualized by taking the difference between the excited state and ground state electron densities and plotting these as areas of decreased (cyan) and increased (purple) electron density (Figure S5). The figure shows that density is transferred from the donor units to the PDI acceptor in the S_1, S_2, and T_2 states, whereas the excited state is mainly localized on the PDI unit for T_1. Furthermore, looking at the natures of the various transitions (Table 2) and the frontier orbital topologies in Figure S3, which include the HOMO-1 and HOMO-2, it is apparent that the HOMO→LUMO and the HOMO-1→LUMO transitions correspond with a charge transfer from the donor to the acceptor, whereas the HOMO-2→LUMO transitions correspond with a more or less localized excited state. The TDDFT calculations using chloroform instead of toluene in the PCM showed only marginal differences (Table S7, S8).

To simulate the UV-Vis absorption spectra and to estimate the energies of the (predominantly) LE states, the calculations were expanded to the third singlet excited state (S_3) for the **BDT**, **DMAC**, and **TPA** containing PDIs and to the fifth singlet excited state (S_5) for **PDI-DTP** (Table S3, S4, S7, S8, Figure S5). The S_3 state shows mixed CT/LE character for **PDI-BDT** and **PDI-TPA**, whereas **PDI-DMAC** shows almost exclusive LE character, presumably due to the higher dihedral angle between the **DMAC** and PDI units. The S_3 and S_4 states of **PDI-DTP** are predominantly of CT character, while the S_5 state is showing a large amount of LE character. The UV-Vis absorption spectra were simulated in toluene (Figure S7) and chloroform (Figure S8) from the results of the TDDFT calculations and show the presence of two distinct absorption peaks corresponding to the

Table 2. Amount of charge-transfer character (q_{CT}) accompanying the $S_0 \rightarrow S_n$ and $S_0 \rightarrow T_n$ transitions in toluene.

PDI	$S_0 \rightarrow S_1$ Nature[a]	q_{CT}[b]	$S_0 \rightarrow S_2$ Nature[a]	q_{CT}[b]	$S_0 \rightarrow T_1$ Nature[a][c]		q_{CT}[b]	$S_0 \rightarrow T_2$ Nature[a]	q_{CT}[b]
BDT	H→L (95%)	0.80	H-1→L (94%)	1.06	H→L (51%)	H-2→L (43%)	0.36	H-1→L (83%)	0.95
DMAC	H→L (94%)	1.10	H-1→L (94%)	1.13	H→L (55%)	H-2→L (40%)	0.56	H-1→L (93%)	1.13
DTP	H→L (90%)	1.01	H-1→L (94%)	1.15	H→L (12%)	H-2→L (59%)	0.36	H→L (74%)	1.12
TPA	H→L (82%)	0.72	H-1→L (90%)	1.08	H→L (41%)	H-2→L (54%)	0.39	H-1→L (76%)	0.96

[a] H = HOMO, L = LUMO. [b] Amount of charge transferred between the indicated states upon excitation. [c] These transitions have both significant H→L and H-2→L character. For **PDI-DTP**, the H-4→L transition also has a significant contribution (24%).

CT (S_1, at longer wavelengths) and LE (S_3 or S_5, at shorter wavelengths) transitions, respectively. The simulated absorption spectra in chloroform (Figure S8) are slightly red-shifted with respect to those in toluene (Figure S7), which is in line with the slightly lower vertical excitation energies obtained in chloroform (Table S7). The transition to the second excited singlet state is not observed because of its negligible oscillator strength (Table 1). Furthermore, the vibronic fine structure observed in the experimental absorption spectra (*vide infra*) is not simulated and hence not visible in Figures S7 and S8.

2.3. Photophysical Characterization

The four new PDI dyads were then subjected to a photophysical investigation to analyze their absorption and emission behavior and to explore their ISC properties by monitoring the generation of $^1O_2$ under illumination at different wavelengths. Chloroform and toluene were selected to screen these properties in a relatively polar and apolar medium, respectively. Absorption and emission spectra afforded the spectral maxima ($\lambda_{abs}(max)$, $\lambda_{em}(max)$) of the absorption and emission bands and the Stokes shifts ($\Delta\bar{\nu}$). Fluorescence quantum yields were obtained at an excitation wavelength of 488 nm, relative to rhodamine 6G, while $^1O_2$ quantum yields were collected by monitoring the absorbance of 1,3-diphenylisobenzofuran (1,3-DPBF) as a $^1O_2$ scavenger during excitation at 525 and 639 nm. All data represented in Table 3 and Figure 2 are mean values from three independent measurements for each compound in the indicated solvent. Only data from the wavelength region of interest are displayed here. For the full absorption spectra, we refer to Figure S9.

As mentioned above, the reported PDI dyes are actually 3:1 mixture of the 1,7- and 1,6-disubstituted regioisomers. The influence of this difference in substitution pattern on the optical properties is described in literature. Somewhat contradictory findings were reported on the possible (non)influence of these isomers.[19,22] However, quantum-chemical calculations indicated the minor influence of the substitution pattern on the energy level distribution of the materials under investigation here (Tables 1, 2, S3–S10). Hence, the resulting photophysical behavior was assumed to be unaffected by the altered bay-substitution pattern.

The absorption profiles exhibit a prominent PDI absorption peak for all dyads in chloroform and toluene solution, accompanied by a higher-wavelength CT absorption band (Figure 2). The localized absorption bands have maxima around 502–510 nm for **PDI-BDT**, **-DMAC**, and **-TPA**, and 460 nm for **PDI-DTP**, which are all hypsochromically shifted with respect to the maximum at 525 nm observed for the pristine N,N′-dialkyl-PDI (Table 3).[23] This blue-shift results from the twisted PDI core due to bay-substitution (Figure S1), a feature frequently encountered in π-system distorted PDI dyes.[1a] The intramolecular CT character is apparent for all PDI compounds, showing relatively intense CT absorption bands, especially for the **BDT**, **DTP**, and **TPA** containing PDIs. Furthermore, a broadening of the localized absorption band is observed for **PDI-BDT**, **PDI-TPA**, and **PDI-DTP** due to the increased electronic coupling between the donor and acceptor as the dihedral angle is relatively smaller (Table 1).[11h] This observation is consistent with the mixed CT/LE character of the S_3 state for **PDI-BDT** and **PDI-TPA**, and the S_5 state for **PDI-DTP**. In **PDI-DMAC**, the donor and acceptor are more orthogonal, which is reflected in a less intense CT band and was also predicted by the low oscillator strength (Table 1). The sharper localized absorption consisting

Table 3. Spectroscopic data for **PDI-BDT**, **PDI-DMAC**, **PDI-DTP**, and **PDI-TPA** as obtained in chloroform and toluene solution.[a]

PDI	Solvent	$\lambda_{abs,LE}$ $\lambda_{abs,CT}$ [nm][b]	$\lambda_{em,LE}$ $\lambda_{em,CT}$ [nm][c]	$\Delta\bar{\nu}_{LE}$ $\Delta\bar{\nu}_{CT}$ [cm^{-1}][d]	Φ_f[e]	$\Phi_{\Delta,525}$[f]	$\Phi_{\Delta,639}$[g]
BDT	chloroform	509 587	529 702	743 2801	0.01 ± 0.00	0.73 ± 0.04	0.76 ± 0.12
	Toluene	502 577	531 668	1070 2376	0.11 ± 0.00	0.80 ± 0.07	0.86 ± 0.04
DMAC	chloroform	510 648	521 _[h]	426 _[h]	0.01 ± 0.01	0.16 ± 0.02	0.07 ± 0.03
	Toluene	507 649	518 796	400 2858	< 0.01	0.26 ± 0.05	0.18 ± 0.04
DTP	chloroform	461 576	544 _[h]	3310 _[h]	0.01 ± 0.00	0.35 ± 0.09	0.13 ± 0.02
	Toluene	460 570	545 _[h]	3397 _[h]	0.01 ± 0.00	0.38 ± 0.04	0.26 ± 0.02
TPA	chloroform	507 626	544 806	1329 3571	< 0.01	0.03 ± 0.01	0.03 ± 0.01
	Toluene	503 626	546 739	1549 2434	0.06 ± 0.00	0.06 ± 0.00	0.04 ± 0.01

[a] Spectrograde chloroform and toluene were used for all measurements. [b] Absorption maxima for the localized and charge-transfer band. [c] Emission maxima for the localized and charge-transfer band. [d] Shifts between the localized and charge-transfer absorption and emission maxima, respectively. [e] Fluorescence quantum yield determined *vs* rhodamine 6G ($\Phi_f = 0.94$, $\lambda_{exc} = 488$ nm) in spectrograde ethanol. [f] Singlet oxygen quantum yield determined *vs* rose bengal ($\Phi_\Delta = 0.86$, $\lambda_{exc} = 525$ nm) in spectrograde ethanol by monitoring the absorbance of 1,3-DPBF at 414 nm. [g] Singlet oxygen quantum yield determined *vs* methylene blue ($\Phi_\Delta = 0.52$, $\lambda_{exc} = 639$ nm) in spectrograde ethanol by monitoring the absorbance of 1,3-DPBF at 414 nm. [h] No charge-transfer emission observed.

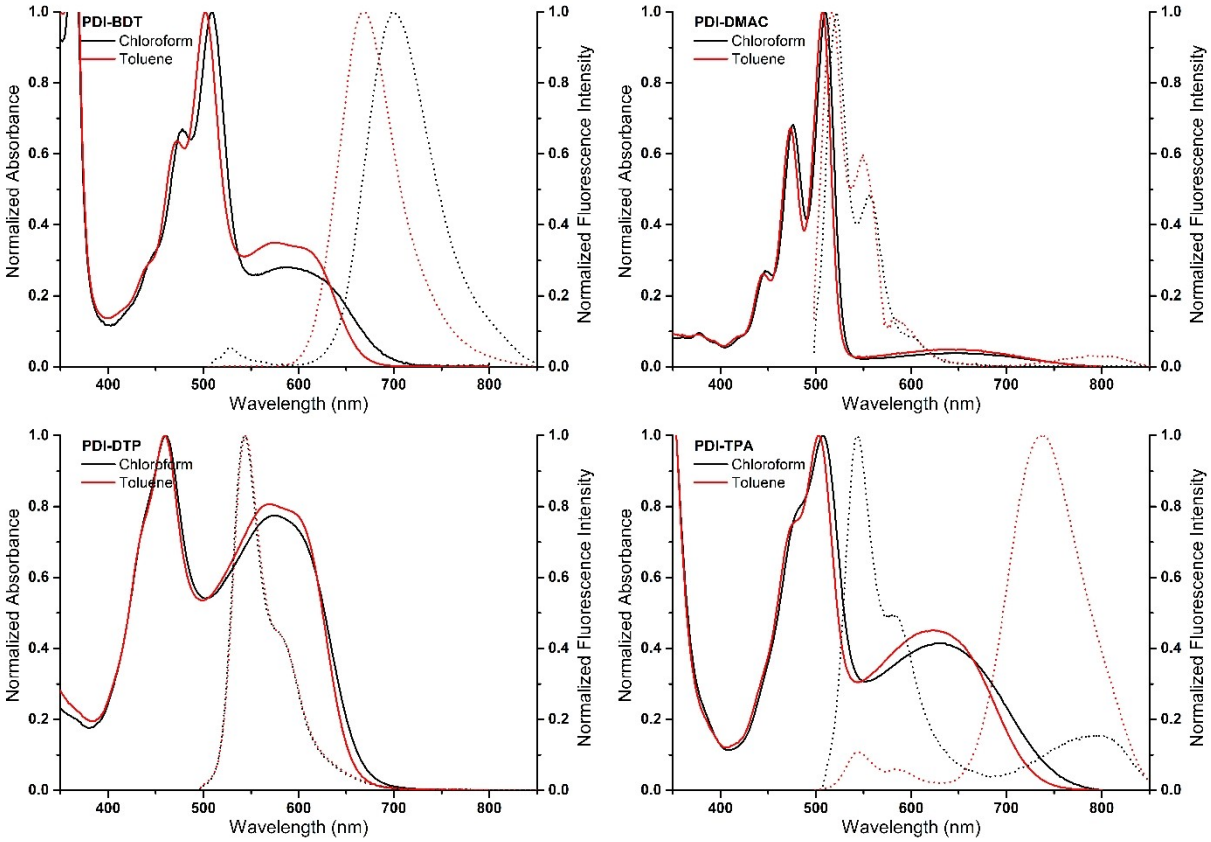

Figure 2. Normalized absorption spectra (solid lines) for **PDI-BDT**, **PDI-DMAC**, **PDI-DTP**, and **PDI-TPA** and their corresponding normalized fluorescence spectra (dashed lines) in chloroform and toluene solution.

of three distinguishable peaks is characteristic to the vibronic fine structure in the $S_0 \rightarrow S_1$ transitions in pure perylene and corresponds to the almost exclusive LE character of the S_3 state.[24] Overall, the experimental (Figure 2) and simulated UV-Vis spectra (Figure S7, S8) are in excellent agreement, in particular with respect to the relative intensity of the (predominantly) LE and CT bands.

The emission behavior depends strongly on the selected donor and the polarity of the surrounding solvent medium (Figure 2, Table 3). The fluorescence profile of **PDI-DMAC** is the mirror image of its absorption, with a small Stokes shift. CT emission is barely visible around 800 nm in toluene and even absent in chloroform. The weak donor-acceptor electronic coupling results in a pronounced vibronic fine-structure of the LE band typical to the PDI core.[24] CT emission is also lacking for **PDI-DTP**, despite the strong CT absorption. Here, only a broadened localized emission band is observed in chloroform and toluene, with a large Stokes shift. The opposite is true for **PDI-BDT**, where CT emission is far more intense than localized emission. Here, solvent polarity is also reflected in the position of the CT emission band. When increasing solvent polarity, the highly polar CT state is stabilized, resulting in a bathochromic shift (34 nm) and broadening of the CT band, accompanied by a decrease in Φ_f.[25] The same trend is seen for **PDI-TPA**. The CT emission band is located at longer wavelengths, as expected from the more red-shifted CT absorption. Notable is the difference in relative intensity of the localized and CT emission bands. Whereas in chloroform the localized perylene emission peak is most intense, the CT band is far more distinct in toluene solution. As the parent PDI is characterized by a near-unity Φ_f, the fluorescence quenching is striking in our donor-acceptor dyads. This is indeed true for all donors, resulting in meager Φ_f values in chloroform. For **PDI-BDT** and **PDI-TPA**, these values are somewhat higher in toluene (0.11 and 0.06, respectively).

Singlet oxygen formation was then evaluated under illumination at 525 nm, revealing very different values depending on the donor moiety (Table 3, Figure 3). In toluene, a high Φ_Δ of 0.80 was obtained for **PDI-BDT**, whereas it was moderate for **PDI-DTP** and even lower for **PDI-DMAC** (0.38 and 0.26, respectively). **PDI-TPA** displayed almost no $^1O_2$ generation ($\Phi_\Delta = 0.06$). In chloroform solution, all values decreased to a slight extent, but similar trends were observed between the different donors. This solvent polarity dependence of Φ_Δ suggests the involvement of CT states in the ISC mechanism. Here, solvent changes will alter the CT state energy, which influences the CT-triplet state energy difference. A better energy alignment could explain the higher $^1O_2$ production in toluene. However, one should consider the increased possibility for CR to the ground state (S_0) as the ^{1}CT energy is decreased in the more polar solvent chloroform. As photoactivity at longer

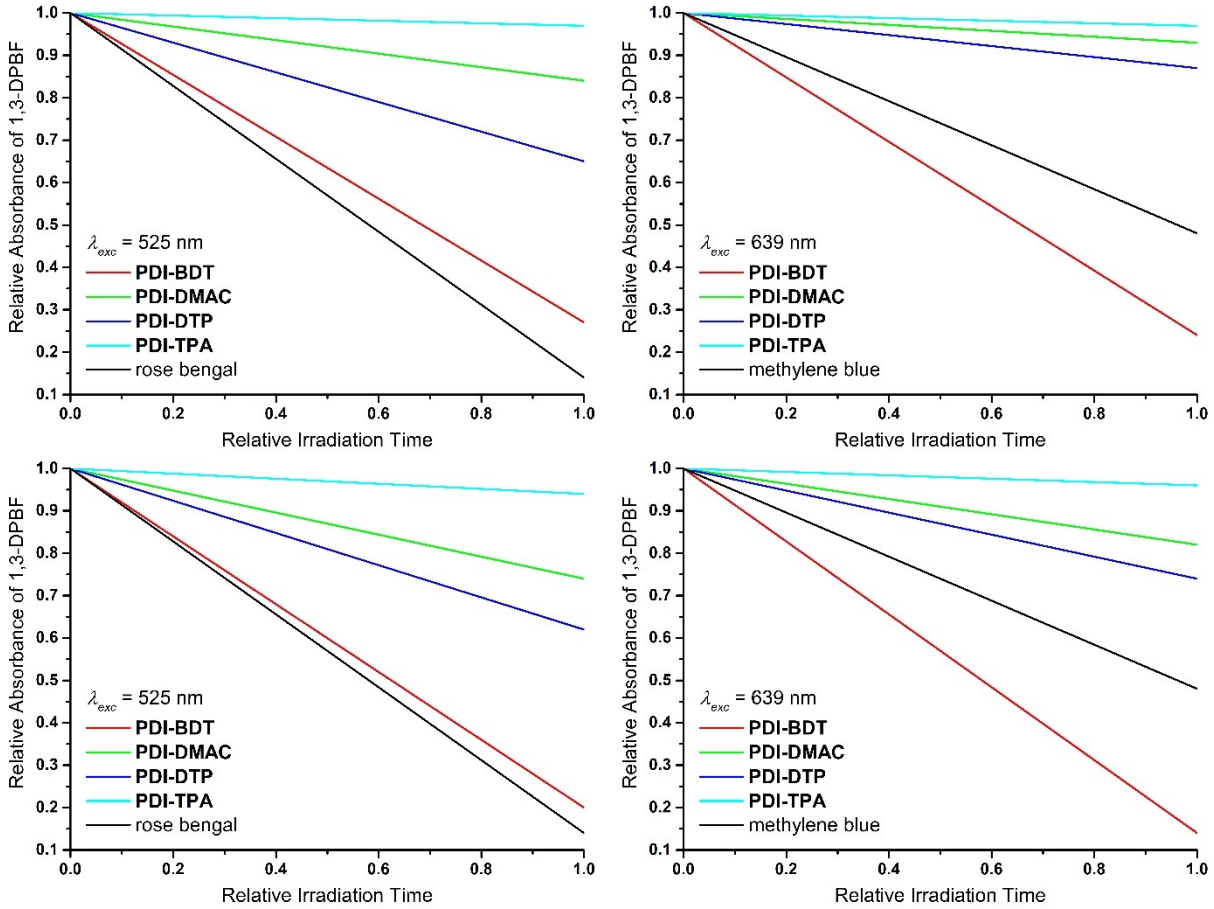

Figure 3. Relative decrease in absorbance of 1,3-diphenylisobenzofuran (1,3-DPBF) at 414 nm under continuous irradiation using a single 525 nm LED (left) or a 639 nm LED (right) in the presence of a PDI dyad in chloroform (top) or toluene (bottom). Rose bengal ($\Phi_\Delta = 0.86$, $\lambda_{exc} = 525$ nm) or methylene blue ($\Phi_\Delta = 0.52$, $\lambda_{exc} = 639$ nm) was used as a standard.

wavelengths is recommended for therapeutic applications, $^1O_2$ production was also investigated at 639 nm (Table 3, Figure 3). Although Φ_Δ values decreased somewhat, they were still significant under this low energy activation. **PDI-BDT** gave even better results, with $\Phi_\Delta = 86\%$ in toluene. Moderate to low Φ_Δ values were obtained for **PDI-DMAC** and **-DTP**, whereas for **PDI-TPA** singlet oxygen production remained very low.

Although ISC was observed indirectly for the donor-PDI dyads through $^1O_2$ generation (Table 3), DFT optimized geometries indicated the absence of a perfect donor-acceptor orthogonality (Table 1), often described as an essential feature in the SOCT-ISC process.[18] However, recently reported PDI dyads showed the same deviation of the perpendicular donor-acceptor orientation, while maintaining efficient SOCT-ISC.[9t,w] To look deeper into the possible pathways for ISC, the quantum-chemical and photophysical analyses were combined. From the quantum-chemical calculations, it can be concluded that the T_1 state is likely too low in energy with respect to S_1 for efficient ISC to occur. Hence, the traditional SOCT-ISC from a CT state to a localized triplet state seems unlikely. T_2, however, is very close in energy to S_1 (Table 1). Both transitions are of CT character and of different nature (HOMO→LUMO for S_1, HOMO-1→LUMO for T_2), making ISC viable according to the El-Sayed rules.[26] The different behavior of the dyads can be explained by looking at the T_2-S_1 energy gaps and the chemical structures of the donor units. The **BDT**, **DMAC**, and **DTP** units are expected to afford a more considerable extent of ISC than the **TPA** moiety because of the smaller T_2-S_1 energy gap, which is apparent from Table 1. As mentioned before, the **BDT** donor is expected to give increased ISC due to the higher SOC associated with the sulfur atoms, which is likely part of the explanation for the high Φ_Δ of 80% in **PDI-BDT** at 525 nm excitation in toluene. Using the same reasoning, **DTP**, which also contains multiple sulfur atoms, should be able to afford significant ISC as well (Table 3). Reduced efficiency for the vibronic coupling between the donor and the acceptor could then possibly explain why it does not reach a high Φ_Δ. **DMAC** gives a negligible energy gap between the T_2 and S_1 states in combination with a larger dihedral angle and is known within the field of TADF to provide good vibronic coupling between the donor and acceptor units in TADF type emitters, explaining why it gives reasonable Φ_Δ values in this work.[13b,e–i] Finally, almost no ISC was observed for **PDI-TPA**, which can be related to the larger T_2-S_1 energy gap in combination with the

rotational freedom of the phenyl rings, resulting in more radiationless energy dissipation.

3. Conclusions

A symmetrical N,N′-substituted perylene diimide (PDI) chromophore was functionalized at its bay-positions with four different donor moieties (benzo[1,2-*b*:4,5-*b*′]dithiophene (**BDT**), 9,9-dimethyl-9,10-dihydroacridine (**DMAC**), dithieno[3,2-*b*:2′,3′-*d*]pyrrole (**DTP**), and triphenylamine (**TPA**)) and the photophysical characteristics of the resulting push-pull dyads were evaluated in solution. Density functional theory optimized geometries revealed the non-orthogonal orientation of the donor units with respect to the PDI acceptor and the deviation from planarity of the PDI core, which explains the hypsochromically-shifted localized absorption and emission. Simulated UV-Vis absorption spectra nicely match the experimental observations. Despite the relatively small dihedral angles ($\theta \leq 76^{\circ}$), singlet oxygen production was demonstrated, revealing intersystem crossing to occur in these heavy-atom-free photosensitizers. Furthermore, direct excitation in the charge-transfer absorption band (at 639 nm) also leads to singlet oxygen generation, thereby opening up possibilities for application in (image-guided) photodynamic therapy. Further time-dependent density functional theory analysis gave more insights into the involved intersystem crossing features. A transition of the first singlet to the second triplet excited state is most likely as both states are of charge-transfer character, of a different nature, and have matching energies. In two cases (**PDI-BDT** and **-DTP**), increased spin-orbit coupling due to the thiophene subunits might assist intersystem crossing, resulting in the highest Φ_{Δ} values (0.80 and 0.38 in toluene at 525 nm, respectively). For the **DMAC** donor, intersystem crossing still occurs ($\Phi_{\Delta} = 0.26$) due to the minimal T_2-S_1 energy difference (~0.00 eV) and increased dihedral angle.

4. Supporting information

Materials and methods, detailed donor-PDI synthesis procedures, additional (TD)DFT data and figures, simulated UV-Vis spectra, full absorption spectra, $^{1}H/^{13}C$ NMR spectra, and coordinates of the optimized geometries can be found in the supporting information.

Acknowledgments

The authors thank Hasselt University and the University of Namur for continuing financial support (BOF Ph.D. scholarships JD and TC). BC and WM thank the Research Foundation-Flanders (FWO) for support through projects G087718N, G0D1521N, I006320N, GOH3816NAUHL, and the Scientific Research Community (WOG) 'Supramolecular Chemistry and Materials' (W000620N). The calculations were performed on the computers of the 'Consortium des équipements de Calcul Intensif (CÉCI)' (http://www.ceci-hpc.be), including those of the 'UNamur Technological Platform of High-Performance Computing (PTCI)' (http://www.ptci.unamur.be), for which we gratefully acknowledge financial support from the FNRS-FRFC, the Walloon Region, and the University of Namur (Conventions No. 2.5020.11, GEQ U.G006.15, U.G018.19, 1610468, and RW/GEQ2016).

Conflict of Interest

The authors declare no conflict of interest.

Keywords: charge transfer · intersystem crossing · perylene diimides · photosensitizers · singlet oxygen

[1] a) C. Huang, S. Barlow, S. R. Marder, *J. Org. Chem.* **2011**, *76*, 2386–2407; b) N. Soh, T. Ueda, *Talanta* **2011**, *85*, 1233–1237; c) M. Sun, K. Müllen, M. Yin, *Chem. Soc. Rev.* **2016**, *45*, 1513–1528; d) F. Würthner, C. R. Saha-Möller, B. Fimmel, S. Ogi, P. Leowanawat, D. Schmidt, *Chem. Rev.* **2016**, *116*, 962–1052; e) F. Fernández-Lázaro, N. Zink-Lorre, Á. Sastre-Santos, *J. Mater. Chem. A* **2016**, *4*, 9336–9346; f) S. Betzold, S. Herbst, A. A. P. Trichet, J. M. Smith, F. Würthner, S. Höfling, C. P. Dietrich, *ACS Photonics* **2017**, *5*, 90–94; g) G. Zhang, J. Zhao, P. C. Y. Chow, K. Jiang, J. Zhang, Z. Zhu, J. Zhang, F. Huang, H. Yan, *Chem. Rev.* **2018**, *118*, 3447–3507; h) A. Nowak-Krol, K. Shoyama, M. Stolte, F. Würthner, *Chem. Commun.* **2018**, *54*, 13763–13772; i) C. Yan, S. Barlow, Z. Wang, H. Yan, A. K. Y. Jen, S. R. Marder, X. Zhan, *Nat. Rev. Mater.* **2018**, *3*, 18003; j) R. Lenaerts, T. Cardeynaels, I. Sudakov, J. Kesters, P. Verstappen, J. Manca, B. Champagne, L. Lutsen, D. Vanderzande, K. Vandewal, E. Goovaerts, W. Maes, *Sol. Energy Mater. Sol. Cells* **2019**, *196*, 178–184.

[2] A. Nowak-Król, F. Würthner, *Org. Chem. Front.* **2019**, *6*, 1272–1318.

[3] H. Langhals, *Heterocycles* **1995**, *40*, 477–500.

[4] W. E. Ford, P. V. Kamat, *J. Phys. Chem.* **1987**, *91*, 6373–6380.

[5] a) S. Fukuzumi, K. Ohkubo, J. Ortiz, A. M. Gutiérrez, F. Fernández-Lázaro, Á. Sastre-Santos, *Chem. Commun.* **2005**, *30*, 3814–3816; b) R. F. Kelley, W. S. Shin, B. Rybtchinski, L. E. Sinks, M. R. Wasielewski, *J. Am. Chem. Soc.* **2007**, *129*, 3173–3181; c) Á. J. Jiménez, F. Spänig, M. S. Rodríguez-Morgade, K. Ohkubo, S. Fukuzumi, D. M. Guldi, T. Torres, *Org. Lett.* **2007**, *9*, 2481–2484; d) A. A. Rachford, S. Goeb, F. N. Castellano, *J. Am. Chem. Soc.* **2008**, *130*, 2766–2767; e) S. Fukuzumi, K. Ohkubo, J. Ortiz, A. M. Gutiérrez, F. Fernández-Lázaro, Á. Sastre-Santos, *J. Phys. Chem. A* **2008**, *112*, 10744–10752; f) E. O. Danilov, A. A. Rachford, S. Goeb, F. N. Castellano, *J. Phys. Chem. A* **2009**, *113*, 5763–5768; g) S. A. Odom, R. F. Kelley, S. Ohira, T. R. Ensley, C. Huang, L. A. Padilha, S. Webster, V. Coropceanu, S. Barlow, D. J. Hagan, E. W. Van Stryland, J.-L. Brédas, H. L. Anderson, M. R. Wasielewski, S. R. Marder, *J. Phys. Chem. A* **2009**, *113*, 10826–10832; h) R. D. Costa, F. J. Céspedes-Guirao, H. J. Bolink, F. Fernández-Lázaro, Á. Sastre-Santos, E. Ortí, J. Gierschner, *J. Phys. Chem. C* **2009**, *113*, 19292–19297; i) M. Supur, M. E. El-Khouly, J. H. Seok, J. H. Kim, K.-Y. Kay, S. Fukuzumi, *J. Phys. Chem. C* **2010**, *114*, 10969–10977; j) M. E. El-Khouly, D. H. Choi, S. Fukuzumi, *J. Photochem. Photobiol. A* **2011**, *218*, 17–25; k) V. L. Gunderson, E. Krieg, M. T. Vagnini, M. A. Iron, B. Rybtchinski, M. R. Wasielewski, *J. Phys. Chem. B* **2011**, *115*, 7533–7540; l) F. N. Castellano, *Dalton Trans.* **2012**, *41*, 8493–8501; m) V. Prusakova, C. E. McCusker, F. N. Castellano, *Inorg. Chem.* **2012**, *51*, 8589–8598; n) M. T. Vagnini, A. L. Smeigh, J. D. Blakemore, S. W. Eaton, N. D. Schley, F. D'Souza, R. H. Crabtree, G. W. Brudvig, D. T. Co, M. R. Wasielewski, *Proc. Natl. Acad. Sci. USA* **2012**, *109*, 15651–15656; o) R. K. Dubey, M. Niemi, K. Kaunisto, K. Stranius, A. Efimov, N. V. Tkachenko, H. Lemmetyinen, *Inorg. Chem.* **2013**, *52*, 9761–9773; p) Y. Wu, Y. Zhen, Z. Wang, H. Fu, *J. Phys. Chem. A* **2013**, *117*, 1712–1720; q) J. Sun, F. Zhong, J. Zhao, *Dalton Trans.* **2013**, *42*, 9595–9605; r) B. A. Llewellyn, A. G. Slater, G. Goretzki, T. L. Easun, X. Z. Sun, E. S. Davies, S. P. Argent, W. Lewis, A. Beeby, M. W. George, N. R. Champness, *Dalton Trans.* **2014**, *43*, 85–94; s) M. Schulze, A. Steffen, F. Würthner, *Angew. Chem. Int. Ed.* **2015**, *54*, 1570–1573; *Angew. Chem.* **2015**, *127*, 1590–1593; t) J. E. Yarnell, I. Davydenko, P. V. Dorovatovskii, V. N. Khrustalev, T. V. Timofeeva, F. N. Castellano, S. R. Marder, C. Risko, S. Barlow, *J. Phys. Chem. C* **2018**, *122*, 13848–13862.

[6] J. Zhao, W. Wu, J. Sun, S. Guo, *Chem. Soc. Rev.* **2013**, *42*, 5323–5351.
[7] a) E. I. G. Azenha, A. C. Serra, M. Pineiro, M. M. Pereira, J. Seixas de Melo, L. G. Arnaut, S. J. Formosinho, A. M. d. A. Rocha Gonsalves, *Chem. Phys.* **2002**, *280*, 177–190; b) J. Zou, Z. Yin, K. Ding, Q. Tang, J. Li, W. Si, J. Shao, Q. Zhang, W. Huang, X. Dong, *ACS Appl. Mater. Interfaces* **2017**, *9*, 32475–32481.
[8] a) J. Zhao, K. Chen, Y. Hou, Y. Che, L. Liu, D. Jia, *Org. Biomol. Chem.* **2018**, *16*, 3692–3701; b) Y. Hou, X. Zhang, K. Chen, D. Liu, Z. Wang, Q. Liu, J. Zhao, A. Barbon, *J. Mater. Chem. C* **2019**, *7*, 12048–12074.
[9] a) E. A. Weiss, M. J. Ahrens, L. E. Sinks, A. V. Gusev, M. A. Ratner, M. R. Wasielewski, *J. Am. Chem. Soc.* **2004**, *126*, 5577–5584; b) E. A. Weiss, M. J. Ahrens, L. E. Sinks, M. A. Ratner, M. R. Wasielewski, *J. Am. Chem. Soc.* **2004**, *126*, 9510–9511; c) F. Yukruk, A. L. Dogan, H. Canpinar, D. Guc, E. U. Akkaya, *Org. Lett.* **2005**, *7*, 2885–2887; d) Z. E. Dance, Q. Mi, D. W. McCamant, M. J. Ahrens, M. A. Ratner, M. R. Wasielewski, *J. Phys. Chem. B* **2006**, *110*, 25163–25173; e) D. Veldman, S. M. Chopin, S. C. Meskers, M. M. Groeneveld, R. M. Williams, R. A. Janssen, *J. Phys. Chem. A* **2008**, *112*, 5846–5857; f) D. Veldman, S. M. Chopin, S. C. Meskers, R. A. Janssen, *J. Phys. Chem. A* **2008**, *112*, 8617–8632; g) E. M. Giacobbe, Q. Mi, M. T. Colvin, B. Cohen, C. Ramanan, A. M. Scott, S. Yeganeh, T. J. Marks, M. A. Ratner, M. R. Wasielewski, *J. Am. Chem. Soc.* **2009**, *131*, 3700–3712; h) M. T. Colvin, E. M. Giacobbe, B. Cohen, T. Miura, A. M. Scott, M. R. Wasielewski, *J. Phys. Chem. A* **2010**, *114*, 1741–1748; i) C. C. Hofmann, S. M. Lindner, M. Ruppert, A. Hirsch, S. A. Haque, M. Thelakkat, J. Kohler, *J. Phys. Chem. B* **2010**, *114*, 9148–9156; j) T. Miura, R. Carmieli, M. R. Wasielewski, *J. Phys. Chem. A* **2010**, *114*, 5769–5778; k) Y. Wu, Y. Zhen, Y. Ma, R. Zheng, Z. Wang, H. Fu, *J. Phys. Chem. Lett.* **2010**, *1*, 2499–2502; l) L. Flamigni, A. Zanelli, H. Langhals, B. Bock, *J. Phys. Chem. A* **2012**, *116*, 1503–1509; m) K. M. Lefler, K. E. Brown, W. A. Salamant, S. M. Dyar, K. E. Knowles, M. R. Wasielewski, *J. Phys. Chem. A* **2013**, *117*, 10333–10345; n) A. J. Tilley, R. D. Pensack, T. S. Lee, B. Djukic, G. D. Scholes, D. S. Seferos, *J. Phys. Chem. C* **2014**, *118*, 9996–10004; o) C. M. Mauck, K. E. Brown, N. E. Horwitz, M. R. Wasielewski, *J. Phys. Chem. A* **2015**, *119*, 5587–5596; p) K. Nagarajan, A. R. Mallia, V. S. Reddy, M. Hariharan, *J. Phys. Chem. C* **2016**, *120*, 8443–8450; q) W. Yang, J. Zhao, C. Sonn, D. Escudero, A. Karatay, H. G. Yaglioglu, B. Küçüköz, M. Hayvali, C. Li, D. Jacquemin, *J. Phys. Chem. C* **2016**, *120*, 10162–10175; r) Z. Yu, Y. Wu, Q. Peng, C. Sun, J. Chen, J. Yao, H. Fu, *Chem. Eur. J.* **2016**, *22*, 4717–4722; s) K. Nagarajan, A. R. Mallia, K. Muraleedharan, M. Hariharan, *Chem. Sci.* **2017**, *8*, 1776–1782; t) N. Rehmat, A. Toffoletti, Z. Mahmood, X. Zhang, J. Zhao, A. Barbon, *J. Mater. Chem. C* **2020**, *8*, 4701–4712; u) X. Zhang, A. A. Sukhanov, E. A. Yildiz, Y. E. Kandrashkin, J. Zhao, H. G. Yaglioglu, V. K. Voronkova, *ChemPhysChem* **2021**, *22*, 55–68; v) F. Sadiq, Z. Wang, Y. Hou, J. Zhao, A. Elmali, D. Escudero, A. Karatay, *Dyes Pigm.* **2021**, *184*, 108708; w) N. Rehmat, I. V. Kurganskii, Z. Mahmood, Q. L. Guan, J. Zhao, Y. H. Xing, G. G. Gurzadyan, M. V. Fedin, *Chem. Eur. J.* **2021**, 27, 5521–5535.
[10] a) Z. E. Dance, S. M. Mickley, T. M. Wilson, A. B. Ricks, A. M. Scott, M. A. Ratner, M. R. Wasielewski, *J. Phys. Chem. A* **2008**, *112*, 4194–4201; b) Y. Zhao, R. Duan, J. Zhao, C. Li, *Chem. Commun.* **2018**, *54*, 12329–12332; c) Y. Hou, T. Biskup, S. Rein, Z. Wang, L. Bussotti, N. Russo, P. Foggi, J. Zhao, M. Di Donato, G. Mazzone, S. Weber, *J. Phys. Chem. C* **2018**, *122*, 27850–27865; d) K. Chen, J. Zhao, X. Li, G. G. Gurzadyan, *J. Phys. Chem. A* **2019**, *123*, 2503–2516; e) M. A. Filatov, *Org. Biomol. Chem.* **2019**, *18*, 10–27; f) M. Imran, A. A. Sukhanov, Z. Wang, A. Karatay, J. Zhao, Z. Mahmood, A. Elmali, V. K. Voronkova, M. Hayvali, Y. H. Xing, S. Weber, *J. Phys. Chem. C* **2019**, *123*, 7010–7024; g) K. Chen, Y. Dong, X. Zhao, M. Imran, G. Tang, J. Zhao, Q. Liu, *Front. Chem.* **2019**, *7*, 821; h) J. Deckers, T. Cardeynaels, H. Penxten, A. Ethirajan, M. Ameloot, M. Kruk, B. Champagne, W. Maes, *Chem. Eur. J.* **2020**, *26*, 15212–15225.
[11] a) L. Fan, Y. Xu, H. Tian, *Tetrahedron Lett.* **2005**, *46*, 4443–4447; b) Z. An, S. A. Odom, R. F. Kelley, C. Huang, X. Zhang, S. Barlow, L. A. Padilha, J. Fu, S. Webster, D. J. Hagan, E. W. Van Stryland, M. R. Wasielewski, S. R. Marder, *J. Phys. Chem. A* **2009**, *113*, 5585–5593; c) H. Wonneberger, C. Q. Ma, M. A. Gatys, C. Li, P. Bäuerle, K. Müllen, *J. Phys. Chem. B* **2010**, *114*, 14343–14347; d) M. J. Lin, B. Fimmel, K. Radacki, F. Würthner, *Angew. Chem. Int. Ed.* **2011**, *50*, 10847–10850; *Angew. Chem.* **2011**, *123*, 11039–11042; e) A. Keerthi, S. Valiyaveettil, *J. Phys. Chem. B* **2012**, *116*, 4603–4614; f) R. Mishra, P. Panini, J. Sankar, *Org. Lett.* **2014**, *16*, 3994–3997; g) L. George, Z. Ahmed, H. Lemmetyinen, A. Efimov, *Eur. J. Org. Chem.* **2015**, *2015*, 584–590; h) Y. Zhao, X. Li, Z. Wang, W. Yang, K. Chen, J. Zhao, G. G. Gurzadyan, *J. Phys. Chem. C* **2018**, *122*, 3756–3772; i) R. Regar, R. Mishra, P. K. Mondal, J. Sankar, *J. Org. Chem.* **2018**, *83*, 9547–9552.
[12] K. Deng, C. Li, S. Huang, B. Xing, D. Jin, Q. Zeng, Z. Hou, J. Lin, *Small* **2017**, *13*, 1702299.
[13] a) J. Gibson, A. P. Monkman, T. J. Penfold, *ChemPhysChem* **2016**, *17*, 2956–2961; b) P. L. Dos Santos, J. S. Ward, M. R. Bryce, A. P. Monkman, *J. Phys. Chem. Lett.* **2016**, *7*, 3341–3346; c) M. K. Etherington, J. Gibson, H. F. Higginbotham, T. J. Penfold, A. P. Monkman, *Nat. Commun.* **2016**, *7*, 13680; d) T. J. Penfold, E. Gindensperger, C. Daniel, C. M. Marian, *Chem. Rev.* **2018**, *118*, 6975–7025; e) R. Furue, K. Matsuo, Y. Ashikari, H. Ooka, N. Amanokura, T. Yasuda, *Adv. Opt. Mater.* **2018**, *6*, 1701147; f) N. A. Kukhta, H. F. Higginbotham, T. Matulaitis, A. Danos, A. N. Bismillah, N. Haase, M. K. Etherington, D. S. Yufit, P. R. McGonigal, J. V. Gražulevičius, A. P. Monkman, *J. Mater. Chem. C* **2019**, *7*, 9184–9194; g) F. M. Xie, H. Z. Li, G. L. Dai, Y. Q. Li, T. Cheng, M. Xie, J. X. Tang, X. Zhao, *ACS Appl. Mater. Interfaces* **2019**, *11*, 26144–26151; h) S. Kothavale, W. J. Chung, J. Y. Lee, *J. Mater. Chem. C* **2020**, *8*, 7059–7066; i) C. Zhou, W.-C. Chen, H. Liu, X. Cao, N. Li, Y. Zhang, C.-S. Lee, C. Yang, *J. Mater. Chem. C* **2020**, *8*, 9639–9645.
[14] T. Cardeynaels, S. Paredis, A. Danos, D. Vanderzande, A. P. Monkman, B. Champagne, W. Maes, *Dyes Pigm.* **2021**, *186*, 109022.
[15] W. Vanormelingen, J. Kesters, P. Verstappen, J. Drijkoningen, J. Kudrjasova, S. Koudjina, V. Liegeois, B. Champagne, J. Manca, L. Lutsen, D. Vanderzande, W. Maes, *J. Mater. Chem. A* **2014**, *2*, 7535–7545.
[16] C. D. Schmidt, N. Lang, N. Jux, A. Hirsch, *Chem. Eur. J.* **2011**, *17*, 5289–5299.
[17] a) F. Würthner, V. Stepanenko, Z. Chen, C. R. Saha-Möller, N. Kocher, D. Stalke, *J. Org. Chem.* **2004**, *69*, 7933–7939; b) P. Rajasingh, R. Cohen, E. Shirman, L. J. Shimon, B. Rybtchinski, *J. Org. Chem.* **2007**, *72*, 5973–5979.
[18] Z. R. Grabowski, K. Rotkiewicz, W. Rettig, *Chem. Rev.* **2003**, *103*, 3899–4032.
[19] a) M. J. Ahrens, M. J. Tauber, M. R. Wasielewski, *J. Org. Chem.* **2006**, *71*, 2107–2114; b) H. Y. Tsai, C. W. Chang, K. Y. Chen, *Molecules* **2013**, *19*, 327–341.
[20] a) T. Cardeynaels, S. Paredis, J. Deckers, S. Brebels, D. Vanderzande, W. Maes, B. Champagne, *Phys. Chem. Chem. Phys.* **2020**, *22*, 16387–16399; b) T. J. Penfold, *J. Phys. Chem. C* **2015**, *119*, 13535–13544.
[21] T. Le Bahers, C. Adamo, I. Ciofini, *J. Chem. Theory Comput.* **2011**, *7*, 2498–2506.
[22] a) R. K. Dubey, A. Efimov, H. Lemmetyinen, *Chem. Mater.* **2011**, *23*, 778–788; b) N. V. Handa, K. D. Mendoza, L. D. Shirtcliff, *Org. Lett.* **2011**, *13*, 4724–4727; c) S. Dey, A. Efimov, H. Lemmetyinen, *Eur. J. Org. Chem.* **2012**, *2012*, 2367–2374; d) R. K. Dubey, M. Niemi, K. Kaunisto, A. Efimov, N. V. Tkachenko, H. Lemmetyinen, *Chem. Eur. J.* **2013**, *19*, 6791–6806.
[23] F. Würthner, *Chem. Commun.* **2004**, 1564–1579.
[24] G. Boobalan, P. M. Imran, S. Nagarajan, *Superlattices Microstruct.* **2012**, *51*, 921–932.
[25] H. Heitele, P. Finckh, S. Weeren, F. Poellinger, M. E. Michel-Beyerle, *J. Phys. Chem.* **1989**, *93*, 5173–5179.
[26] a) M. A. El-Sayed, *J. Chem. Phys.* **1963**, *38*, 2834–2838; b) M. Baba, *J. Phys. Chem. A* **2011**, *115*, 9514–9519.

Manuscript received: April 8, 2021
Revised manuscript received: May 10, 2021
Accepted manuscript online: May 25, 2021
Version of record online: June 15, 2021